American Journal of Physical Chemistry
2025, Vol. 14, No. 2, pp. 23-32
https://doi.org/10.11648/j.ajpc.20251402.12

Research Article

Synthesis and Characterisation of Sudan Red-G/Cyclodextrin Doped ZnO Nanocrystals

Palanichamy Ramasamy[1], Ayyadurai Mani[2], Balakrishnan Sneha[1], Ezhil Nivetha[1], Albert Antony Muthu Prabhu[3], Govindaraj Venkatesh[4], Narayanasamy Rajendiran[1, *]

[1]Department of Chemistry, Annamalai University, Annamalai Nagar, India
[2]Center for Advanced Energy Materials, SRM TRP Engineering College, Tiruchy, India
[3]Department of Chemistry, Aditanar College of Arts and Science, Tiruchendur, India
[4]Department of Chemistry, Knowledge Institute of Technology (Autonomous), Salem, India

Abstract

Sudan Red-G/cyclodextrin-doped zinc oxide nanocrystals are synthesized and characterized by UV-visible, fluorescence, FTIR, DTA, XRD, SEM, and TEM methods. Solvent and cyclodextrin studies confirm the existence of the azo-hydrazo tautomer in the SRG molecule. The ground and excited state absorption wavelengths of SRG are similar to Red G, Sudan I, and Sudan II. The dipole moment, internal energy, free energy, enthalpy, entropy, and the HOMO-LUMO energy levels of SRG, α-CD, β-CD, SRG/α-CD, and SRG/β-CD are determined using the PM3 method. SRG's horizontal bond length is higher than the α-CD and β-CD cavity size, only a partial inclusion of the SRG molecule occurs in the CD. Absorption and emission spectral shifts are largely varied when SRG/CD doped on ZnO. Compared to SRG and ZnO/β-CD, the ZnO/SRG/β-CD nanocrystals showed significant differences in the FTIR, DTA and XRD peaks, indicating that SRG and β-CD were successfully doped onto the ZnO nanoparticles. TEM morphology supports the formation of nanocrystals in the SRG/CD doped ZnO. The nanocrystal sizes are analyzed using TEM-EDS and XRD techniques.

Keyword

Sudan Red-G, Zinc Oxide Nano, Cyclodextrin, Tautomerism, Nanocrystals

1. Introduction

Zinc oxide nanoparticles (ZnO NPs) generally used in various fields like rubber, textile, concrete, sensors, photocatalysis, photoelectron devices, electronics, highly functional and effective devices, electrotechnology, antibacterial and antimicrobial industries [1-18]. It has been used considerably for its catalytic, electrical, optoelectronic, and photochemical properties. In rubber industry, ZnO NPs was used due to their ability to improve the wear resistance of rubber composites, increase the strength and durability of high polymers, and prevent aging, among other advantages [4, 5]. ZnO is also

*Corresponding author: drrajendiran1967@gmail.com (Narayanasamy Rajendiran)

Received: 17 April 2025; **Accepted:** 27 April 2025; **Published:** 20 June 2025

incorporated into personal care products like sunscreens and cosmetics for its effective UV light absorption properties [6]. An addition of ZnO NPs in the textile industry, the fabrics imparts deodorization, antibacterial activity, and resistance to UV and visible light [7]. Since zinc oxide shows different physical and chemical properties depending upon the morphology of nano structures, not only various synthesis methods but also the physical, chemical and spectral properties of synthesized zinc oxide are to be investigated in terms of its morphology. The applications and characteristics of ZnO nano are analysed with other metal oxides, but no work is done with drugs and dyes. Because of this reason, this manuscript focuses on: a) investigating the presence of intramolecular hydrogen bonding (IHB) or azo-hydrazo tautomer in SRG; b) synthesizing and characterizing ZnO, ZnO/CD, ZnO/SRG, and ZnO/SRG/CD nanomaterials using various spectral and microscopic techniques; and c) studying the impact of doping SRG/CD onto ZnO nanoparticles.

2. Experimental

2.1. Preparation of SRG/CD

1, 2, 4, 6, 8, and 10 mL of 0.01 M α-CD and β-CD aqueous solutions were added to a 10 mL standard measuring flask (SMF). After adding 0.2 mL of SRG (2×10^{-2} M), the solution was diluted with triple-distilled water to a final volume of 10 mL. The final SRG concentration in each flask was 4×10^{-4} M, and the α-CD and β-CD concentrations varying from 0.1×10^{-2} M to 1.0×10^{-2} M.

2.2. Preparation of ZnO and ZnO/SRG/CD Nanomaterials

0.01 M zinc sulfate was dissolved in 100 mL of deionized water and heated at 50–60 ℃ for 20–30 minutes. A 1:2 molar ratio of $ZnSO_4$ and NaOH was prepared, and the solution was vigorously stirred for 12 hours at 300 K. After several washings, the white ZnO precipitate was separated by centrifugation [19-23]. The precipitate was then dried at 100 ℃ for six hours and the final size range of ZnO nanoparticles are 25–50 nm.

SRG (20 mL of 2×10^{-3} M) was mixed with CD (80 mL of 1×10^{-2} M) in a reaction vessel. Zinc sulfate (100 mL of 0.01 M) was then added to the mixture and heated at 50 ℃ for one hour. Then, 2-5 mL of 1 M NaOH was introduced, and the mixture was stirred for 1–2 hours. The mixture was then freeze-dried and dehydrated at -80 ℃. The resulting ZnO/SRG/CD powder was collected and used for spectral microscopic analysis.

2.3. Molecular Modeling Studies

The ground-state geometry of SRG, α-CD, β-CD, SRG/α-CD, and SRG/β-CD in the gas phase was optimized using the PM3 method and Gaussian 09W software [23, 34]. The initial geometries of the SRG and CD molecules were constructed with Spartan 08 and then optimised by the PM3 method. α-CD and β-CD were fully optimised by PM3 without any symmetry constraints. Because the semi-empirical PM3 method has been shown to be a powerful tool in the conformational study of Guest: CD complexes and has high computational efficiency in calculating CD systems it was selected to study the inclusion process of CD with SRG in this work.

3. Result and Discussion

3.1. Influence of Solvents, α-CD, and β-CD on SRG

Absorption and fluorescence bands of Sudan Red-G (SRG, 2-[(E)-(2-methoxyphenyl) diazenyl] naphthalen-2-ol, Figure 1) were analysed in various solvents, α-CD and β-CD (Table 1, and Figure 2). SRG exhibited four absorption peaks in all the solvents, α-CD, and β-CD, and the position and shape of the spectra are similar to those of Sudan I (SDI), Sudan II (SDII), and Sudan Red B (SRB) [23, 24]. The absorption and fluorescence spectra of SRG in cyclohexane were blue-shifted (λ_{abs} ~ 490, 311, 262, 229 nm, λ_{emi} ~ 573, 350 nm) compared to SDI (λ_{abs} ~ 502, 465, 434, 336, 305, 236 nm, λ_{emi} ~ 582, 350 nm), SDII (λ_{abs} ~ 516, 489, 426, 310, 230 nm, λ_{emi} ~ 589, 355 nm), and SRB (λ_{abs} ~ 510, 350, 239 nm, λ_{emi} ~ 582, 377 nm). The trend in the ground state wavelength is SRG < SDI < SRB < SDII. This sequence indicates that the ground and excited state behavior is primarily influenced by the location of the substituents on the aromatic ring.

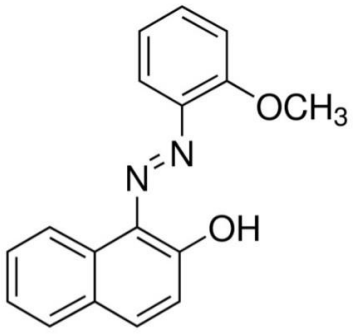

Figure 1. *Chemical structure of Sudan Red-G [SRG].*

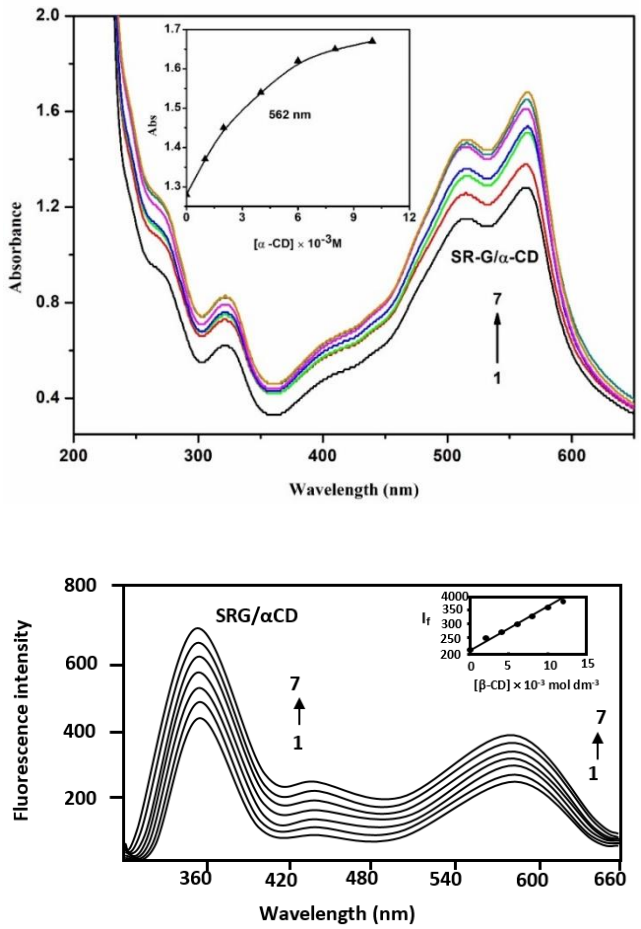

Figure 2. *Absorption and fluorescence spectra of SRG in different α-CD concentrations (M): (1) 0, (2) 0.001, (3) 0.002, (4) 0.004, (5) 0.006, (6) 0.008, (7) 0.01. Insert figure: absorbance/ IF vs [α-CD].*

In the excited state, SRG are bathochromic shifted from cyclohexane to water. Notably, compared to cyclohexane, in neutral pH-7, the ground state absorption maxima of SRG (λ_{abs}~ 562, 514, 322, 268 nm, λ_{emi}~ 587, 350 nm) experience a more significant red shift due to the formation of hydroxyl anions. The ground state absorption bands are broader, stronger, and exhibit a pronounced bathochromic shift due to interactions between the OH/OCH_3 groups and the -N=N- group. The variations observed in the ground and excited states in all the solvents and the CD solutions suggest that the SRG molecule is encapsulated within the CD cavity. The larger bathochromic shift observed for SRG, SDI, SDII, and SRB is attributed to the enhanced charge movement effect among the hydroxyl/ methoxy groups and the phenyl/naphthalene rings. These shifts, either bathochromic or hypsochromic, indicate greater resonance exchanges of the azo group and the aromatic ring [13-20]. When α-CD and β-CD concentrations increased, the absorption wavelength of SRG slightly shifted from 562, 514, 322, 268 nm to 564, 516, 323, 268 nm (Figure 2). SRG exhibited multiple emission in aqueous and CD solutions (344, 424, and 587 nm) and intensities were increased at the same wavelength. In the S_0 and S_1 states, the spectral changes of SRG in water, and CDs are similar suggesting that both α-CD, and β-CD form similar guest-host complexes with SRG [23-33].

Table 1. *Absorption and fluorescence spectral maxima of SRG with different solvents, α-CD and β-CD.*

Solvents	λ_{abs}	log ε	λ_{flu}
Cyclohexane	490	3.22	
	311	2.58	573
	262	2.95	350
	229	3.42	
1,4-Dioxane	490	3.22	
	311	2.58	572
	262	2.95	350
	229	3.46	
Ethyl acetate	490	3.25	
	312	2.77	574
	262	3.06	350
	250	3.05	
Acetonitrile	492	3.28	
	310	2.77	576
	262	3.06	350
	231	3.43	
2-Propanol	503	3.27	
	312	2.78	580
	261	3.08	350
	245	3.07	
Ethanol	503	3.27	
	312	2.70	579
	261	3.01	350
	228	3.51	
Water	562	3.82	
	514	3.78	587
	322	3.50	350
	268	3.68	
α-CD (0.01 M)	564	3.94	
	516	3.89	588
	323	3.63	424
	268	3.81	343
β-CD (0.01 M)	561	3.73	588
	513	3.68	424

Solvents	λ_{abs}	log ε	λ_{flu}
	321	3.42	343
	268	3.65	
Excitation wavelength (nm)	-	-	510 320

In SRG, the broad band and significant bathochromic shifts observed in the S_0 and S_1 states suggest the presence of an intramolecular hydrogen bond (IHB) (Table 1 and Figure 2). Specifically, the ortho -OH and the -N=N- groups form a six-membered ring through IHB. The maxima in both states remain largely unchanged across solvents of varying polarities, which supports the presence of the azo-hydrazo tautomeric form in SRG [13, 14, 24-30]. In comparison to other solvents, water shows a decrease in emission intensity at the shorter wavelength (350 nm) and an increase at the longer wavelength (583 nm). These observations indicate that as solvent polarity increases, the "hydrazo" form becomes more dominant, while the "azo" form decreases [23, 24]. In contrast to hydroxyl groups, methoxy substituents have negligeable effect on the azo-hydrazo tautomer (Table 1). These findings suggest: i) the hydroxyl group in SRG induces significant bathochromic shifts in both tautomeric forms in the ground state; ii) the position of the functional group within the phenyl/naphthalene ring plays a critical role in determining the ground and excited state behavior, and iii) the methoxy group does not impact the wavelength of the azo-hydrazo tautomer.

Bathochromic shifts observed for the longest ground state wavelength in the tautomeric forms of SRG (Table 1) are primarily attributed to the donor OH group. Similar effects have been noted in Sudan Red-B, SDI, and SDII [13, 14]. Additionally, the band positions in the ground state are largely independent of solvent polarity, with only small shifts observed, further suggesting the existence of the azo-hydrazo tautomer. These results also imply that in polar solvents, the donor OH group stabilizes the hydrazo tautomer [34-41].

3.2. Computational Study

The S_0 state structure of SRG, α-CD, β-CD, SRG/α-CD, and SRG/β-CD were optimized by PM3 method (Figure 3). Table 2 provides the dipole moment, internal energy, free energy, enthalpy, entropy, HOMO, and LUMO values for these systems [23, 34]. Using two different coordinate sets, the optimization was initialized by positioning either an anisole or naphthol ring of the SRG towards the CD cavity. The height of the α-CD and β-CD is 7.8 Å, while the interior diameter of the α-CD and β-CD is 5.6 and 6.5 Å respectively. The horizontal and vertical bond distances of SRG are 9.21 Å and 6.08 Å respectively. Since the SRG's horizontal bond length exceeds the α-CD and β-CD cavity size, a partial inclusion of the SRG molecule only happens. Hydrogen bonds formed between the hydroxyl groups of the CDs further stabilize the 1: 1 guest/host complexes. This stabilization leads to variations in the ground and excited-state intensities of SRG in both the CD and solvent environments. The optimized inclusion complex structures confirm partial embedding of SRG in the CD cavity.

The ΔE, ΔH, ΔG, and ΔS values for the most stable SRG/α-CD and SRG/β-CD inclusion complexes are listed in Table 2. In comparison to isolated CDs and SRG/α-CD, the above values for the SRG/β-CD inclusion complex are more negative, signifying greater stability. The negative ΔH and ΔG values indicate that the inclusion complex formation is both exothermic and spontaneous.

Table 2. *Energetic features, thermodynamic parameters and HOMO-LUMO energy calculations for SRG and its inclusion complexes by semiempirical PM3 method.*

Properties	SRG	α-CD	β-CD	SRG/α-CD	SRG/β-CD
E_{HOMO} (eV)	-8.45	-10.37	-10.35	-8.52	-8.80
E_{LUMO} (eV)	-0.53	1.26	1.23	-0.73	-1.06
$E_{HOMO} - E_{LUMO}$ (eV)	7.92	-11.63	-11.58	7.78	7.73
Dipole (D)	1.49	11.34	12.29	11.80	12.39
E (kcal mol^{-1})	31.49	-1247.62	-1457.63	-1219.58	-1434.92
ΔE (kcal mol^{-1})	-	-	-	-3.45	-8.78
G (kcal mol^{-1})	183.46	-676.37	-789.52	-861.77	-975.00
ΔG (kcal mol^{-1})	-	-	-	-1.94	-16.48
H (kcal mol^{-1})	140.40	-570.84	-667.55	-727.99	-824.43
ΔH (kcal mol^{-1})	-	-	-	-16.75	-2.02

Properties	SRG	α-CD	β-CD	SRG/α-CD	SRG/β-CD
S (kcal/mol-Kelvin)	0.144	0.353	0.409	0.448	0.505
ΔS (kcal/mol-Kelvin)	-	-	-	0.049	0.049
ZPE	171.41	635.09	740.56	807.86	-913.72

kcal/mol; **kcal/mol-Kelvin; ZPE = Zero-point vibration energy

The HOMO-LUMO energy gaps for SRG/α-CD and SRG/β-CD suggest that significant variations will occur in the electronic structure, inclusion, and binding of SRG. In the HOMO and LUMO diagrams, green and red colors represent positive and negative phases of the molecule, respectively, while blue color indicates nitrogen atoms. The molecular electrostatic potential (MEP) map (Figure 3) shows a red region, indicating a higher electronegative charge compared to other atoms. Larger values of (EHOMO-ELUMO) generally indicate greater stability. When compared to the SRG molecule, the SRG/β-CD inclusion complex has a more negative HOMO-LUMO gap, reflecting its enhanced stability.

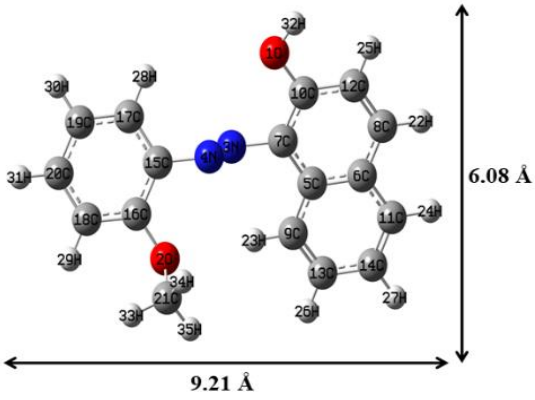

(a) PM3 optimized structure for SRG

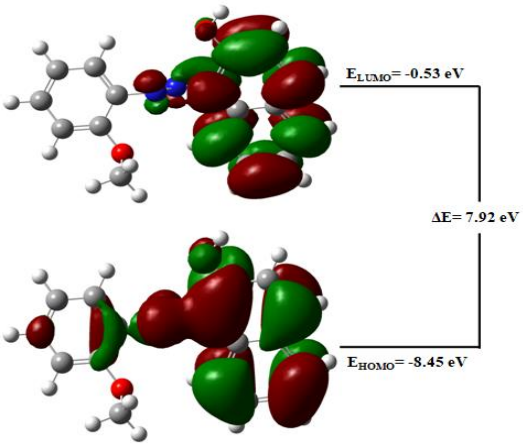

(c) HOMO, LUMO

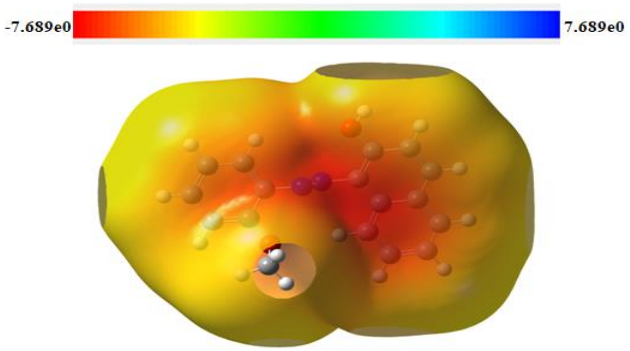

(d) MEP

Figure 3. PM3 optimized structures of (a) SRG (b) HOMO, LUMO and (c) MEP of SRG.

3.3. Effect of SRG/β-CD Doping on ZnO Nanoparticles

The ground and excited states wavelength of the ZnO, ZnO/SRG, ZnO/β-CD, and ZnO/SRG/β-CD nanoparticles were examined. ZnO nano exhibit absorption and emission peaks at 320 nm and 420 nm, and 355 nm, respectively. It is well known that factors such as nanoparticle size, shape, metal type, and surrounding environment can influence spectral bands, and that the particle count does not correlate with the intensity of spectral maxima [23]. When the SRG molecule is incorporated into ZnO nanoparticles, the UV-visible and fluorescence maxima shift to 560 nm, 507 nm, 323 nm, and 575 nm, 410 nm, respectively. When β-CD doped on ZnO nano, the UV-visible and fluorescence wavelengths shift to 250 nm and 398 nm, respectively. When both SRG and β-CD are incorporated into ZnO nanoparticles, the UV-visible maxima shift to 367 nm and 257 nm, while the fluorescence maximum moves to 460 nm and 370 nm, respectively. These variations in UV-visible and fluorescence shifts indicate that SRG and CD have been successfully doped onto the ZnO nano.

3.4. FE-SEM and TEM Morphology

The morphologies of SRG, ZnO nanoparticles, ZnO/β-CD, and ZnO/SRG/β-CD nanocrystals were examined using

FE-SEM and EDAX (Figure 4). ZnO nanoparticles were observed to form small spherical clusters. ZnO/β-CD appeared as sheet-like structures, while SRG had a brick-shaped form. on the other hand, ZnO/SRG/β-CD exhibited a nanorod morphology. The FE-SEM-EDAX analysis revealed the following elemental compositions: (a) ZnO nanoparticles consisted of 57.34% zinc and 42.66% oxygen, (b) ZnO/β-CD nanoparticles contained 19.67% zinc, 54.42% oxygen, and 25.91% carbon, (c) SRG was composed of 69.18% carbon, 9.93% nitrogen, and 20.89% oxygen, and (d) the ZnO/SRG/β-CD nanoparticles had 45.08% zinc, 22.68% carbon, 1.95% nitrogen, and 30.29% oxygen. The variations in the images and atomic percentages of ZnO, SRG, and ZnO/SRG/β-CD nanocrystals indicate the formation of new nanostructures.

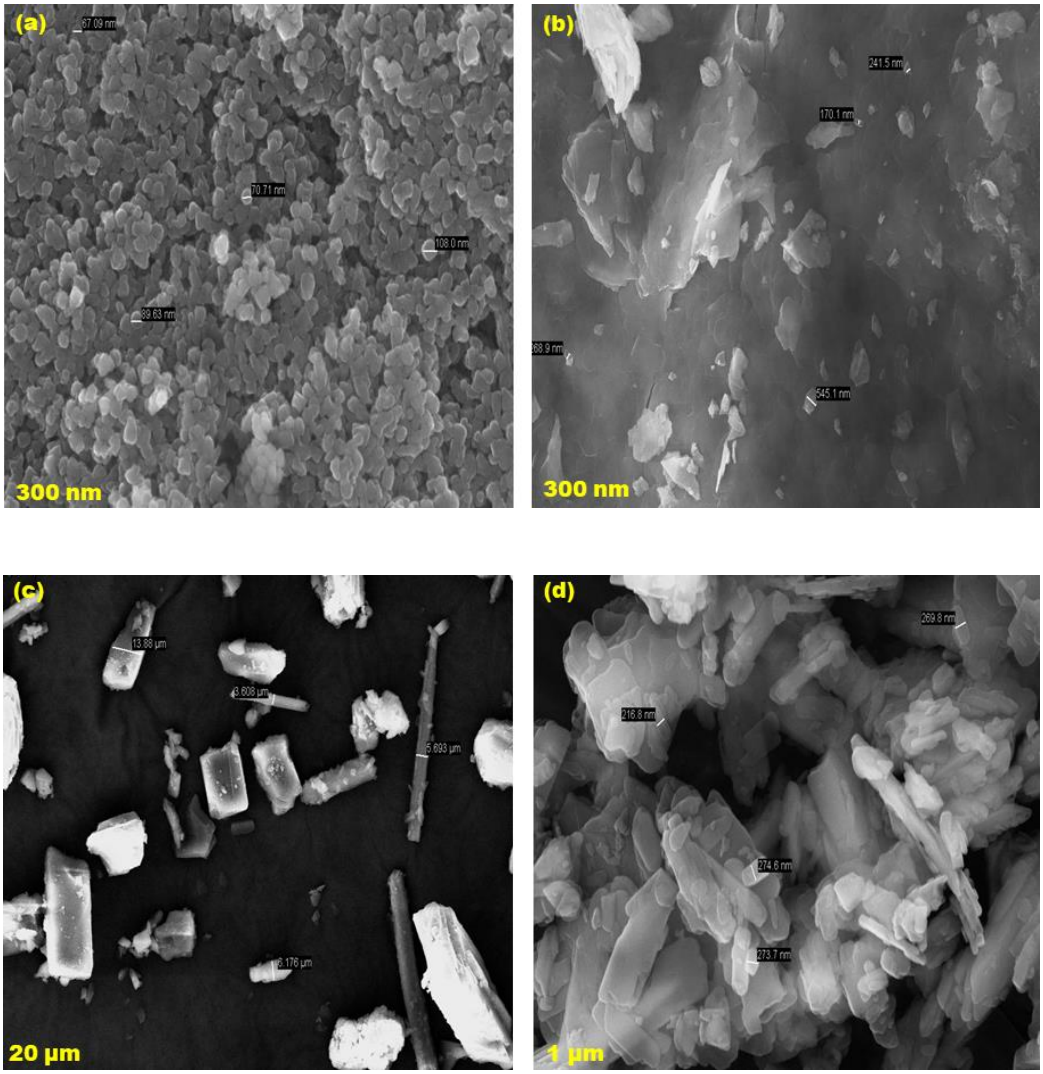

Figure 4. *FE-SEM images for (a) ZnO, (b) ZnO/β-CD, (c) SRG, (d) ZnO/SRG/β-CD.*

TEM illustrate the morphologies (Figure 5) of the above nanomaterials. ZnO nanoparticles exhibited a sheet-like structure, while ZnO/β-CD appeared rod-shaped, and ZnO/SRG/β-CD displayed stone-like particles ranging from 16 to 24 nm. The TEM images revealed that ZnO nanosheets were globular particles with sizes between 20 and 44 nm, while ZnO/β-CD nano ranged from 20 to 40 nm. TEM-EDX data further supported the development of the ZnO/SRG/β-CD nanoparticles: (a) ZnO nano contained 69.84% zinc and 30.16% oxygen, (b) ZnO/β-CD contained 8.79% zinc, 44.59% oxygen, and 46.61% carbon, and (c) ZnO/SRG/β-CD had 75.09% zinc, 13.24% carbon, 10.67% oxygen, and 1.00% nitrogen. These findings confirmed the formation of the ZnO/SRG/β-CD nano.

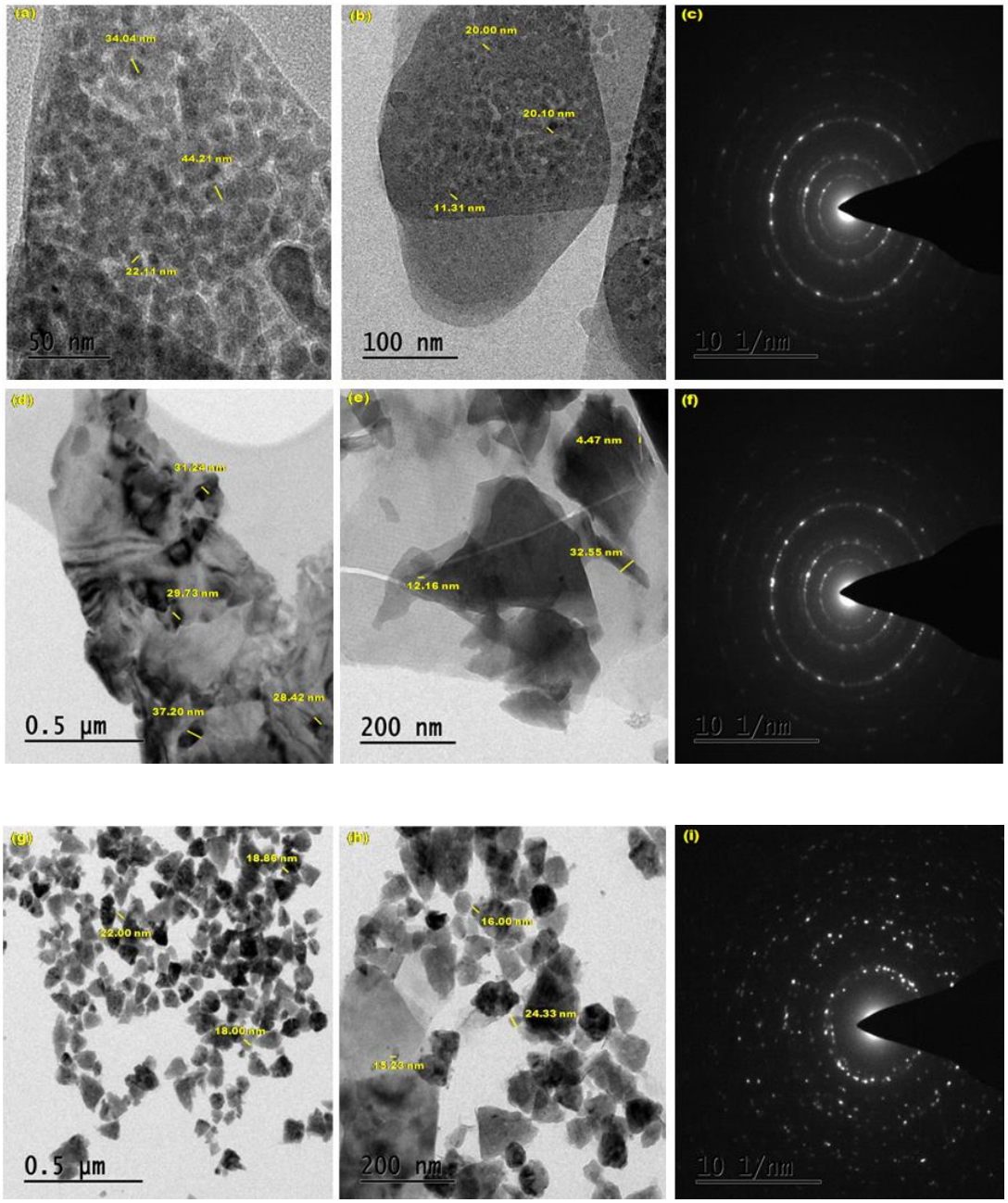

Figure 5. *HR-TEM images for (a-c) ZnO, (d-f) ZnO/β-CD, (g-i) ZnO/SRG/β-CD.*

HR-TEM measurements indicated sizes of 24.98 nm for ZnO, 23.98 nm for ZnO/β-CD, and 19.06 nm for ZnO/SRG/β-CD. XRD results showed the following particle sizes: ZnO at 19.30 nm, β-CD at 23.84 nm, SRG at 21.68 nm, ZnO/β-CD at 20.69 nm, and ZnO/SRG/β-CD at 15.80 nm. A comparison of the XRD and HR-TEM methods revealed a size variation of approximately 3-4 nm between the two techniques.

3.5. Powder X-RD Method

For this study, JCPDS card number 03-065-3411 and data card number 800-075 were utilized. The XRD peaks of the samples were compared to the standard ZnO face-centered cubic (fcc) peaks. The observed hkl planes included (100), (002), (101), (102), (103), (110), (112), and (201). ZnO nanoparticles and β-CD displayed eight XRD peaks at 31.80, 34.51, 36.21, 47.52, 56.61, 62.90, 67.91, 69.92 and 13.39, 19.93, 23.50, 27.65, 31.96, 35.54, 40.58, 48.90, respectively. In the ZnO/β-CD sample, ten peaks were observed at 10.15, 15.18, 25.41, 28.38, 34.92, 42.29, 49.77, 59.16, 63.32, and 70.33. SRG exhibited eight peaks at 12.32, 24.72, 27.69, 32.94, 35.09, 41.43, 50.32, and 61.24. ZnO/SRG/β-CD showed eight peaks at 10.05, 14.90, 25.40, 28.37, 32.94, 41.84, 58.55, and 62.86. Compared to SRG and β-CD, the ZnO/SRG/β-CD nanocrystals displayed a different diffraction pattern and varied peak intensities, indicating the formation of new nanocrystals. Additionally, several prominent peaks

between 10° and 80° confirmed the synthesis of ZnO/SRG/β-CD nanocrystals.

3.6. FT-IR Studies

FTIR analysis was conducted on ZnO nanoparticles, SRG, ZnO/SRG, ZnO/β-CD, and ZnO/SRG/β-CD. The ZnO nanoparticles showed characteristic peaks at 3325, 1587, 1450, 592, and 513 cm^{-1}, with the peaks at 3325, 592, and 513 cm^{-1} confirming the presence of ZnO nanoparticles [13, 23]. When ZnO was combined with β-CD, the peak at 3325 cm^{-1} shifted to 3280 cm^{-1}, the 1587 and 1450 cm^{-1} peaks shifted to 1614 and 1514 cm^{-1}, and the 592 and 513 cm^{-1} peaks shifted to 594 and 526 cm^{-1}, suggesting interaction between ZnO nanoparticles and β-CD.

In SRG, the OH and OCH_3 groups produced peaks at 3255 and 2843 cm^{-1}, the azo group appeared at 1390 cm^{-1}, and the phenyl ring was identified by peaks at 1608 and 1552 cm^{-1}. Other notable peaks included the C-OH group at 2348 cm^{-1}, out-of-plane C-H vibrations at 839 and 744 cm^{-1}, and the C-N-C bond at 586 cm^{-1}. When ZnO nanoparticles were added to SRG/β-CD, the positions of these peaks shifted slightly. In the ZnO/SRG/β-CD composite, the OH peak remained at 3255 cm^{-1}, the OCH_3 peak weakened, the -N=N- group peak shifted to 1384 cm^{-1}, and the aromatic ring peaks moved to 1606 and 1550 cm^{-1}. The C-OH peak appeared at 2350 cm^{-1}, the out-of-plane C-H peaks were at 837 and 746 cm^{-1}, and the C-N-C peak shifted to 596 cm^{-1}. When compared to SRG and ZnO/β-CD, the ZnO/SRG/β-CD nanocrystals showed significant differences in the FTIR peaks, indicating that SRG and β-CD were successfully doped onto the ZnO nanoparticles.

3.7. DTA Thermogram

DTA analysis was performed on ZnO nanoparticles, SRG, ZnO/β-CD, and ZnO/SRG/β-CD. ZnO nanoparticles exhibited two exothermic peaks at 226.1 ℃ and 546.7 ℃, and three endothermic peaks at 272.6 ℃, 731.1 ℃, and 919.2 ℃. SRG showed two exothermic peaks at 289.8 ℃ and 841.9 ℃, with one endothermic peak at 183.5 ℃, while β-CD displayed a single exothermic peak at 128.6 ℃. In the ZnO/β-CD sample, two exothermic peaks were observed at 224.3 ℃ and 932.4 ℃, along with four endothermic peaks at 265.2 ℃, 354.6 ℃, 749.8 ℃, and 884.1 ℃. The ZnO/SRG/β-CD composite exhibited two endothermic peaks at 295.5 ℃ and 964.8 ℃, and four exothermic peaks at 235.7 ℃, 470.7 ℃, 748.6 ℃, and 1017.1 ℃. The endothermic peaks observed in all cases are attributed to the loss of water from the materials. The differences in the endothermic and exothermic peak patterns in SRG, ZnO, β-CD, and ZnO/SRG/β-CD confirm the formation of new nanocrystals.

4. Conclusion

Sudan Red-G/cyclodextrin-doped zinc oxide nanocrystals are synthesized and characterized by UV-visible, fluorescence, FTIR, DTA, XRD, SEM, and TEM methods. The presence of the azo-hydrazo tautomer in the SRG molecule is validated through solvent and CD analysis. The ground and excited state absorption wavelengths of SRG are similar to Red G, Sudan I, and Sudan II. The dipole moment, internal energy, free energy, enthalpy, entropy, and the HOMO-LUMO energy levels of SRG, α-CD, β-CD, SRG/α-CD, and SRG/β-CD are determined using the PM3 method. SRG's horizontal bond length is higher than the α-CD and β-CD cavity size, only a partial inclusion of the SRG molecule occurs in the CD. Absorption and emission spectral shifts are largely varied when SRG/CD doped on ZnO. Compared to SRG and ZnO/β-CD, the ZnO/SRG/β-CD nanocrystals showed significant differences in the FTIR, DTA and XRD peaks, indicating that SRG and β-CD were successfully doped onto the ZnO nanoparticles. TEM morphology supports the formation of nanocrystals in the SRG/CD ‘doped ZnO. Both XRD and TEM data indicated that the size of the nanocrystals ranged from 16 to 35 nm.

Abbreviations

FTIR	Fourier Transform Infrared Spectroscopy
DTA	Differential Thermal Analysis
XRD	X-ray Diffraction
SEM	Scanning Electron Microscopy
TEM	Transmission Electron Microscopy
HOMO	Highest Occupied Molecular Orbital
LUMO	Lowest Unoccupied Molecular Orbital
SRG	Sudan Red G
ZnO NPs	Zinc Oxide Nanoparticles
α-CD	Alpha Cyclodextrin; β-CD – Beta Cyclodextrin
SDI	Sudan I
SDII	Sudan II
SRB	Sudan Red B
PM3	Parametric Method 3
ΔE	Internal Energy Change
ΔH	Enthalpy Change
ΔG	Free Energy Change
ΔS	Entropy Change

Acknowledgments

This work was supported by the Rashtriya Uchchatar Shiksha Abhiyan (RUSA) Phase -2.0 [No. 128/A1/ RUSA 2.0, Health and Environment] New Delhi, India.

Author Contributions

Narayanasamy Rajendiran: Supervision, Writing –

original draft, Writing – review & editing

Ayyadurai Mani: Data curation, Investigation

Govindaraj Venkatesh: Software, Validation

Conflicts of Interest

The authors declare no conflicts of interest.

References

[1] Mishra PK, Mishra H, Ekielski A, Talegaonkar S, Vaidya B, Zinc oxide nanoparticles: a promising nanomaterial for biomedical applications. *Drug Discovery Today. 2017;* 22: 1825–1834. https://doi.org/10.1016/j.drudis.2017.08.006

[2] Smijs TG, Pavel S, Titanium dioxide and zinc oxide nanoparticles in sunscreens: focus on their safety and effectiveness. *Nanotechnology, Science and Applications. 2011;* 4: 95–112. PMCID: PMC3781714 PMID: 24198489.

[3] Ruszkiewicz JA, Pinkas A, Ferrer B, Peres TV, Tsatsakis A, Aschner M, Neurotoxic effect of active ingredients in sunscreen products, a contemporary review. *Toxicology Reports. 2017;* 4: 245–259. https://doi.org/10.1016/j.toxrep.2017.05.006

[4] Kolodziejczak-Radzimska A, Jesionowski T, Zinc oxide–from synthesis to application: a review. *Materials. 2014;* 7: 2833–2881. https://doi.org/10.3390/ma7042833

[5] Sahoo S, Maiti M, Ganguly A, George JJ, Bhowmick AK, Effect of zinc oxide nanoparticles as cure activator on the properties of natural rubber and nitrile rubber. *J Applied Polymer Science. 2007;* 105: 2407–2415. https://doi.org/10.1002/app.26296

[6] Newman M D, Stotland M, llis JI, The safety of nanosized particles in titanium dioxide- and zinc oxide based sunscreens. *J American Academy of Dermatology. 2009;* 61: 685–692. https://doi.org/10.1016/j.jaad.2009.02.051

[7] Amir Hatamie, Azam Khan, Mohsen Golabi, Anthony PF Turner, Valerio Beni, Wing Cheung Mak, Azar Sadollahkhani, Hatim Alnoor, Behrooz Zargar, Sumaira Bano, Omer Nur, Magnus Willander, Zinc oxide nanostructure-modified textile and its application to biosensing, photocatalysis, and as antibacterial material. *Langmuir. 2015;* 31: 10913–10921. https://doi.org/10.1021/acs.langmuir.5b02341

[8] Xiao FX, Hung SF, Tao HB, Miao J, Yang HB, Liu B, Spatially branched hierarchical ZnO nanorod-TiO_2 nanotube array heterostructures for versatile photocatalytic and photo electrocatalytic applications: towards intimate integration of 1D-1D hybrid nanostructures. *Nanoscale. 2014;* 6: 14950–14961. https://doi.org/10.1039/C4NR04886E

[9] Joshi, SS, Patil, PR, Naimase, MS, Bakare, PP: Role of ligands in the formation, phase stabilization, structural and magnetic properties of α-Fe_2O_3 nanoparticles. *J. Nanopart. Res. 2006;* 5: 635–643. https://doi.org/10.1007/s11051-005-9033-x

[10] Cheng, XL, Zhao, H, Huo, LH, Gao, S, Zhao, JG, ZnO nanoparticulate thin film: preparation, characterization and gas-sensing properties. *Sens. Actuators B. 2004;* 102: 248–252. https://doi.org/10.1016/j.snb.2004.04.080

[11] Lee, SY, Shim, ES, Kang, HS, Pang, SS: Fabrication of ZnO thin film diode using laser annealing. *Thin Solid Films. 2005;* 437: 31–34. https://doi.org/10.1016/j.tsf.2004.06.194

[12] Wang, ZL, Kong, XY, Ding, Y, Gao, P, Hughes, WL: Semiconducting and piezoelectric oxide nanostructures induced by polar surfaces. *Adv. Funct. Mater. 2004;* 14: 943–956. https://doi.org/10.1002/adfm.200400180

[13] Huang, YH, Zang, Y, Liu, L, Fan, SS, Wei, Y, He, J: Controlled synthesis and field emission properties of ZnO nanostructures with different morphologies. *J. Nanosci. Nanotechnol. 2006;* 6: 787–790. https://doi.org/10.1166/jnn.2006.086

[14] Brida, D, Fortunato, E, Ferreira, I, Aguas, H, Martins, R: New insights on large area flexible position sensitive detectors. *J. Non-Cryst. Solids. 2002;* 299: 1272–1276. https://doi.org/10.1016/S0022-3093(01)01092-4

[15] Wang, ZL: Zinc oxide nanostructures: growth properties and applications. *J. Phys. Condens. Matter. 2004;* 16: R829–R858. https://doi.org/10.1088/0953-8984/16/25/R01

[16] Suchea, M, Christoulakis, S, Moschovis, K, Katsarakis, N, Kiriakidis, G: ZnO transparent thin films for gas sensor applications. *Thin Solid Films. 2006;* 515: 551–554. https://doi.org/10.1016/j.tsf.2005.12.295

[17] Ashour, A, Kaid, MA, El-Syed, NZ, Ibrahim, AA: Physical properties of ZnO thin films deposited by spray pyrolysis technique. *Appl. Surf. Sci. 2006;* 252: 7844–7848. https://doi.org/10.1016/j.apsusc.2005.09.048

[18] Chen, JC, Tang, CT: Preparation and application of granular ZnO/Al_2O_3 catalyst for the removal of hazardous trichloroethylene. *J. Hazard. Mater. 2007;* 142: 88–96. https://doi.org/10.1016/j.jhazmat.2006.07.061

[19] Cristina Ş Iosub, Elena Olăreț, Alexandru Mihai Grumezescu, Alina M Holban, Ecaterina Andronescu, Toxicity of nanostructures—a general approach. *Nanostructures for Novel Therapy, Elsevier, 2017;* 793–809. https://doi.org/10.1016/b978-0-323-46142-9.00029-3

[20] Noorian SA, Hemmati Nejad N, Navarro JA, Ligand modified cellulose fabrics as support of zinc oxide nanoparticles for UV protection and antimicrobial activities. *International J biological macromolecules. 2020;* 154: 1215-1226. https://doi.org/10.1016/j.ijbiomac.2019.10.276

[21] Noorian SA, Hemmati Nahid N, Bashari Azadeh, One-Pot Synthesis of Cu_2O/ZnO Nanoparticles at Present of Folic Acid to Improve UV-Protective Effect of Cotton Fabrics. *Photochem and Photobiol. 2015;* 91: 510–517. https://doi.org/10.1111/php.12420

[22] Marina E Vance, Todd Kuiken, Eric P Vejerano, Sean P McGinnis, Michael F Hochella Jr, David Rejeski, Matthew S Hull, Nanotechnology in the real world: Redeveloping the nanomaterial consumer products inventory. *Beilstein J Nanotech. 2015;* 6: 1769–1780. https://doi.org/10.3762/bjnano.6.181

[23] Prema Kumari, J, Antony Muthu Prabhu, A, Venkatesh, G, Subramanian, VK, Rajendiran, N, Effect of solvents and pH on β-CD Inclusion complexation of 2,4-dihydroxy azobenzene and 4-hydroxy azobenzene. *J. Solution Chemistry,* 2011; 40: 327–347. https://doi.org 10.1007/s10953-010-9639-1

[24] Antony Muthu Prabhu A, Venkatesh G, Rajendiran N, Azo-Hydrazo tautomerism in 1-phenyazo-2-naphthol dyes in various solvents, pH and β-CD. *J Fluorescence* 2010; 20: 961–972. https://doi.org/10.1007/s10895-010-0642-0

[25] Antony Muthu Prabhu A, Venkatesh G, Sankaranarayanan RK, Rajendiran N, Azonium-ammonium tautomerism and inclusion complexation of 4-amino-2', 3-dimethyl azobenzene. *Indian J Chem*, 2010; 49A: 407–417.

[26] Venkatesh G, Antony Muthu Prabhu A, Rajendiran N, Azonium-Ammonium Tautomerism and Inclusion Complexation of 1-(2,4-diamino phenylazo) naphthalene and 4-Amino azobenzene. *J. Fluorescence.* 2011; 21: 1485-1497. https://doi.org/10.1007/s10895-011-0835-1

[27] Rajendiran N, Sankaranarayanan RK, Azo dye/cyclodextrin: New findings of identical nanorods through 2:2 inclusion complexes. *Carbohydrate Polymers.* 2014; 106: 422–431. https://doi.org/10.1016/j.carbpol.2014.01.030

[28] Venkatesh G, Rajendiran N, Cyclodextrin-Covered Organic Microrods and Micro sheets Derived from Supramolecular Self Assembly of 2,4-Dihydroxy azobenzene and 4-Hydroxy azobenzene Inclusion Complexes. *Bull Chem Soc Jpn* 2014; 87: 283-293. https://https://doi.org/10.1246/bcsj.20130255

[29] Rajendiran N, Sankaranarayanan RK, Venkatesh G, Encapsulation of thiazolyl azoresorcinol and thiazolyl azocresol dyes with a- and b-cyclodextrin cavities: Spectral and molecular modeling studies. *J Mol Struc* 2014; 1072: 242–252. https://doi.org/10.1016/j.molstruc.2014.05.018

[30] Ramasamy P, Mani A, Sneha B, Nivetha E, Venkatesan M, Rajendiran N, Azo-hydrazo tautomerism in Sudan Red-B and Cyclodextrin/ Sudan Red-B doped ZnO nanomaterials J Molecular Structure 1329 (2025) 141423-32. https://doi.org/10.1016/j.molstruc.2025.141423

[31] Mani A, Ramasamy P, Antony Muthu Prabhu A, Rajendiran N, Investigation of Ag and Ag/Co bimetallic nanoparticles with naproxen-cyclodextrin inclusion complex**.** *J. Molecular Structure* 2023; 1284: 135301-10*,* https://doi.org/10.1016/j.molstruc.2023.135301

[32] Mani A, Venkatesh G, Senthilraja P, Rajendiran N, Synthesis and Characterisation of Ag-Co-Venlafaxine-Cyclodextrin Nanorods. *European J Advanced Chemistry Research,* 2024; 5: 9-16. https://doi.org/10.24018/ejchem.2024.5.1.147

[33] Mani A, Ramasamy P, Antony Muthu Prabhu A, Senthilraja P, Rajendiran N, Synthesis and Analysis of Ag/Olanzapine /Cyclodextrin and Ag/Co/Olanzapine /Cyclodextrin Inclusion Complex Nanorods. *Physics and Chemistry of Liquids,* 2024; 62: 196-209. https://doi.org/10.1080/00319104.2023.2297223

[34] A. Mani, P. Ramasamy, A. Antony Muthu Prabhu, P. Senthilraja and N. Rajendiran, Synthesis and Characterisation of Ag/Co/Chloroquine/Cyclodextrin Inclusion Complex Nanomaterials *J Sol-Gel Science and Technology*, in press 2005. https://doi.org/10.1007/s10971-024-06620-5

[35] Antonov L, Fabian FMW, Taylor JP Tautomerism in some aromatic Schiff bases and related azo compounds: an LSER study. J Phys Org Chem 2005; 18: 1169-75. https://doi.org/10.1002/poc.965

[36] Antonov L, Nedeltcheva D Resolution of overlapping UV–Vis absorption bands and quantitative analysis. *Chem Soc Rev.* 2000; 29: 217-227. https://doi.org/10.1039/a900007k

[37] Fabian WMF, Antonov L, Nedeltcheva D, Kamounan FS, Taylor PJ Tautomerism in Hydroxy naphthaldehyde Anils and Azo Analogues: A Combined Experimental and Computational Study. *J Phys Chem A.* 2004; 108: 7603-7612. https://doi.org/10.1021/jp048035z

[38] Zollingser H, Colour chemistry, Synthesis, properties and applications of organic dyes and pigments. 1st Edition, Weinheim, New York 2005.

[39] Joshi H, Kamounah FS, Gooijer C, van der Zwan G, Antonov L, Excited state intramolecular proton transfer in some tautomeric azo dyes and schiff bases containing an intramolecular hydrogen bond. *J Photochem Photobiol A Chem*. 2002; 152: 183-191. https://doi.org/10.1016/S1010-6030(02)00155-7

[40] L. Antonov, Walter M. F. Fabian, Daniela Nedeltcheva, Fadhil S. Kamounah, Tautomerism of 2-hydroxynaphthaldehyde Schiff bases. *J. Chem. Soc. Perkin Trans.* 2, 2000; 1173-79.

[41] Gilli P, Bertolasi V, Pretto L, Lycka A, Gilli G, The Nature of Solid-State N−H···O/O−H···N Tautomeric Competition in Resonant Systems. Intramolecular Proton Transfer in Low-Barrier Hydrogen Bonds Formed by the O ═ C−C ═ N−NH···⇄ ···HO−C ═ C−N ═ N··· Ketohydrazone−Azoenol System. A Variable-Temperature X-ray Crystallographic and DFT Computational Study. *J Am Chem Soc*. 2002; 124: 13554-67. https://doi.org/10.1021/ja020589x